Tellus (2002), 54A, 485–496
Printed in UK. All rights reserved

TELLUS
ISSN 0280–6495

Impact of polar vortex variability on the wintertime low-level climate of east Antarctica: results of a regional climate model

By M. R. VAN DEN BROEKE[1]* and N. P. M. VAN LIPZIG[2]†, [1]*Institute for Marine and Atmospheric Research, Utrecht University, PO Box 80005, 3508 TA Utrecht, The Netherlands;* [2]*Royal Netherlands Meteorological Institute, The Netherlands*

(Manuscript received 5 October 2001; in final form 13 June 2002)

ABSTRACT

Observations show that wintertime low level wind and temperatures in East Antarctica respond markedly to variations in the Southern Hemisphere circumpolar vortex. To explain this, we use output of a regional climate model RACMO/ANT1. A strong vortex extends far to the south and to relatively low atmospheric levels, which reduces the strength and directional constancy of the low-level easterlies. Over the ocean, the easterlies south of the circumpolar pressure trough (CPT) are significantly weakened and the westerlies north of it enhanced. Over the ice sheet, an increased katabatic forcing counteracts the weakening of the easterly near-surface winds. Together with the increased background temperature gradient, which enhances west-to-east turning of the large scale winds, the wind effects of vortex variability over the East Antarctic ice sheet are limited. Pronounced temperature effects are found on the ice sheet: under strong vortex conditions the lower troposphere over East Antarctica cools by 1–3 K through decreased meridional exchange of air. In addition, the weaker low-level easterlies reduce downward mixing of warm air, which causes additional cooling by up to 1.5 K at the surface.

1. Introduction

Climate change in Antarctica (Fig. 1) has not been uniform over the last decades. A 2.5 °C temperature rise occurring in the Antarctic Peninsula over the past 45 yr (King and Harangozo, 1998) has led to the rapid disintegration of some of the Northern Peninsula ice shelves (Vaughan and Doake, 1996; Scambos et al., 2000). In contrast to this, temperature observations in East Antarctica do not show a uniform warming signal (Jones, 1995), and even cooling has recently been reported in some areas (Doran et al., 2002).

Several problems hamper the interpretation of East Antarctic temperature records. The lower troposphere over East Antarctica is characterized by a quasi-permanent temperature deficit (Connolley, 1996) and strong and persistent katabatic winds (Parish and Bromwich 1987) that interact in a complex manner. Moreover, the relatively short East Antarctic temperature records (<50 yr) show large interannual variability that masks possible underlying temperature trends.

Results from recent literature show that an important part of the near-surface variability stems from variations in the strength of the circumpolar vortex in the Southern Hemisphere. About 20 yr ago, Raper et al. (1984) reported on significantly lower station temperatures in East Antarctica when the circumpolar westerlies are strong, which we now know is a manifestation of a strong vortex or the high mode of the Antarctic Oscillation (AAO) (Thompson and Wallace, 2000).

*Corresponding author.
e-mail: broeke@phys.uu.nl
†Present address: British Antarctic Survey, Cambridge, UK.

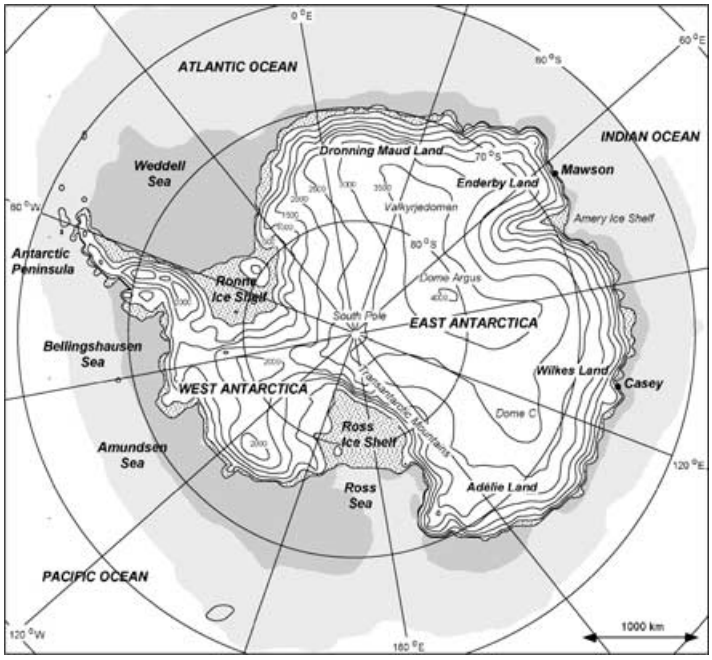

Fig. 1. Model domain and topographical features of Antarctica. Stippled areas, ice shelves, light shaded, average July sea ice extent, dark shaded, average January sea ice extent (from ERA-15). Surface elevation (m asl) is contoured every 500 m.

Indeed, recent temperature trends in Antarctica have been coupled to a persistent positive bias in the AAO index (Thompson and Solomon, 2002), possibly coupled to springtime ozone losses in the stratosphere. This has caused a suppressed amplitude of the semi-annual wave in the Southern Hemisphere (Van Loon, 1967; Meehl et al., 1998; Burnett and McNicoll, 2000) with consequences for Antarctic near-surface temperature trends and the annual cycle (Van den Broeke, 2000a,b).

To illustrate the strong coupling between the polar vortex and the near-surface climate in East Antarctica, Figs. 2a and 2b show July monthly mean 2 m temperature, T_{2m}, and 10 m wind speed, V_{10m}, at two coastal stations, Mawson (67.6°S, 62.9°E) and Casey (66.3°S, 110.5°E), as a function of 500 hPa zonal wind speed, U_{500hPa}. At Mawson/Casey, 68%/71% of the temperature and 54%/34% of the wind speed variations are explained by variations in U_{500hPa}. Note that monthly mean temperature and wind speed of individual July months can differ by as much as 15 °C/ 15 m s^{-1} (Mawson) and 13 °C/ 8 m s^{-1} (Casey). This underscores the very large variability that is observed in the near-surface climate of Antarctica.

In this paper we investigate the coupling between the vortex and low-level climate in East Antarctica by decoupling free atmosphere and near-surface signals. We use output of a regional atmospheric climate model that has been especially adapted for use over Antarctica. A brief model description is given in section 2. Section 3 describes how model results are used to calculate the components of the momentum budget. Results are presented in sections 4 and 5, conclusions in section 6.

2. Model description

The regional climate model RACMO/ANT1 has a domain of 122 × 130 gridpoints covering Antarctica and the surrounding oceans (Fig. 1). At the lateral boundaries, RACMO/ANT1 is forced by ERA15 data (ECMWF reanalysis, 1980–1993). Sea surface temperature and sea ice cover are prescribed from ERA15. Horizontal resolution is ca. 55 km, which enables a reasonably accurate representation of the steep coastal ice slopes and the ice shelves fringing the coast. In the vertical, 20 hybrid levels are used. Compared to the

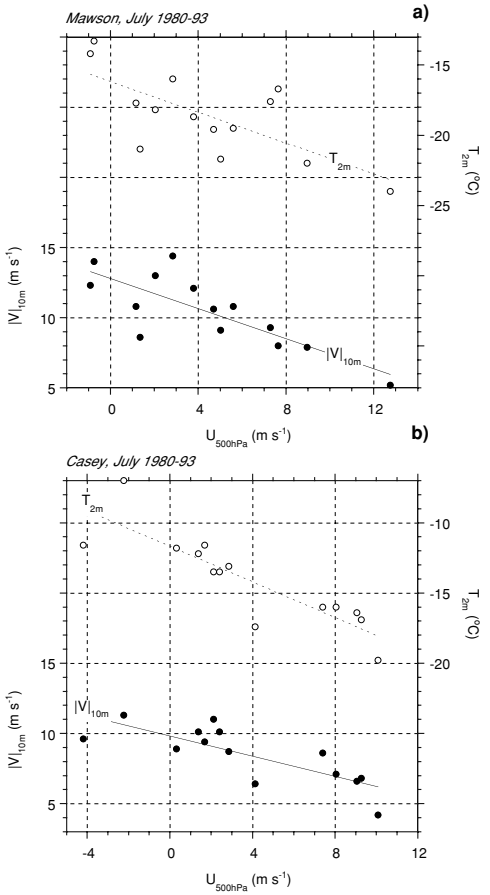

Fig. 2. Observations, July 1980–1993: monthly mean 2 m temperature (open symbols) and 10 m wind speed (filled symbols) as a function of 500 hPa zonal wind, for Mawson (a) and Casey (b).

original model version, several improvements were made with regard to the physical representation of the snow surface (albedo, specific heat and heat conductivity of the snow, and deep snow temperature initialisation; see Van Lipzig, 1999). An additional layer at ca. 7 m above the surface was included to capture better the strong temperature and wind speed gradients near the surface. RACMO/ANT1 is a hydrostatic model. The assumption of hydrostatic balance is acceptable in katabatic flows as long as the horizontal length scales dominate the vertical ones, as is usually the case over the East Antarctic ice sheet (Mahrt, 1982).

In general, the performance of RACMO/ANT1 is a great improvement over earlier models (Van Lipzig et al., 1999), but some problems remain. The surface roughness z_0 is composed of a basic value over snow (set to 1 mm) to which is added a contribution from sub-grid topographical variance. The latter parameterisation leads to overestimated z_0 and underestimated near-surface winds in regions of rough topography (e.g. the Transantarctic Mountains) and, because roughness lengths for heat and moisture z_h and z_q are set equal to z_0, overestimated turbulent exchange of heat and moisture. We have therefore excluded from the present analysis all model gridpoints with $z_0 >$ 1 mm.

3. Methods

3.1. Binning of model data

We use model output from the East Antarctic sector between longitudes 30°W and 180°E where the large-scale circulation and the katabatic winds are more uniform than over West Antarctica and the Antarctic Peninsula. For clarity of presentation, data are binned in nine surface-elevation intervals and six distance intervals over the ocean (Table 1). Over the ice sheet, we use the dowslope/cross-slope coordinate system, while over the ocean the usual west–east coordinate system is adopted (Fig. 3). Note that in July all ocean bins are situated over sea ice.

3.2. Partitioning of TDL and background fields

To seperate the large-scale from boundary-layer effects, we define the temperature deficit layer (TDL), where potential temperature Θ deviates from the backgound value Θ_0 by an amount $\Delta_\Theta (\Delta_\Theta < 0)$. Θ_0 is obtained from downward linear extrapolation of the free atmosphere potential temperature profile towards the surface. An obvious advantage of using the TDL is that we avoid defining the depth of the atmospheric boundary layer, which is poorly constrained in stable conditions.

We define the large-scale wind (U_{LSC}, V_{LSC}) as the geostrophic wind that responds solely to the large-scale pressure gradient. Inside the TDL the actual wind will deviate from (U_{LSC}, V_{LSC}) due to katabatic forcing and thermal wind effects. To calculate (U_{LSC}, V_{LSC}) in the TDL we assume it to be in thermal wind balance with Θ_0:

Table 1. *Some statistics of the 15 bins. Only points were used between 30°W and 180°E longitude and with $z_O = 1$ mm over the ice sheet*

Bin number	Bin characteristic	Bin name	Area (% of total)	Average elevation (m asl)	Average DTC[a] (km)	Average slope (m km^{-1})
1	>3750 m asl	High Interior	1.1	3858	−1299	1.3
2	3250–3750 m asl	Middle Interior	8.2	3492	−994	1.5
3	2750–3250 m asl	Low Interior	10.2	3011	−849	1.9
4	2250–2750 m asl	High Escarpment	8.3	2514	−588	2.3
5	1750–2250 m asl	Middle Escarpment	3.7	2037	−378	4.0
6	1250–1750 m asl	Low Escarpment	2.0	1531	−224	6.3
7	750–1250 m asl	High Coastal	1.4	1009	−125	9.6
8	150–750 m asl	Middle Coastal	1.5	476	−59	11.2
9	0–150 m asl	Low Coastal	2.8	84	0	2.6
10	0–200 km	Coastal Sea	8.0	0	134	0.0
11	200–400 km		9.7	0	302	0.0
12	400–600 km		11.0	0	500	0.0
13	600–800 km		11.0	0	702	0.0
14	800–1000 km		10.9	0	897	0.0
15	1000–1200 km		10.2	0	1098	0.0

[a]DTC = distance to coast.

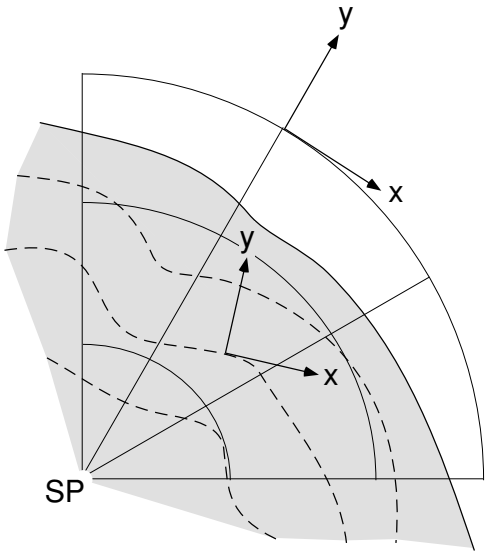

Fig. 3. Orientation of down/cross slope coordinates over the ice sheet (stippled line are schematic height contours) and ordinary W–E and S–N coordinates over the ocean (where slope direction is undefined).

$$\frac{\partial U_{\mathrm{LSC}}}{\partial \ln p} = +\frac{R_{\mathrm{d}}}{f}\left(\frac{p}{p_0}\right)^{\frac{R_{\mathrm{d}}}{c_p}} \frac{\partial \Theta_0}{\partial y}$$

$$\frac{\partial V_{\mathrm{LSC}}}{\partial \ln p} = -\frac{R_{\mathrm{d}}}{f}\left(\frac{p}{p_0}\right)^{\frac{R_{\mathrm{d}}}{c_p}} \frac{\partial \Theta_0}{\partial x}. \qquad (1)$$

Using these expressions, the free atmospheric wind above the TDL can be extrapolated downwards to the surface.

3.3. TDL momentum budget

Having defined Δ_Θ and $(U_{\mathrm{LSC}}, V_{\mathrm{LSC}})$ we can calculate the terms in the budget for mean downslope flow

(V) on an inclined surface of constant slope α with coordinates (x, y, z) orthogonal to the surface (positive y directed down the slope, positive x directed to the right):

$$\underbrace{\frac{\partial V}{\partial t}}_{} = \underbrace{-U\frac{\partial V}{\partial x}}_{\text{ADVH}} \underbrace{- V\frac{\partial V}{\partial y} - W\frac{\partial V}{\partial z}}_{\text{ADVV}} \underbrace{+ \frac{g}{\Theta_0}\frac{\partial \bar{\Theta}}{\partial y}}_{\text{THW}} \underbrace{- fU}_{\text{COR}} \underbrace{+ fU_{\text{LSC}}}_{\text{LSC}} \underbrace{- \frac{\partial \overline{vw}}{\partial z}}_{\text{FDIV}} \underbrace{+ \frac{g}{\Theta_0}\Delta_\Theta \sin\alpha}_{\text{KAT}}$$

where

$$\Delta_\Theta(z) = \Theta(z) - \Theta_0(z)$$

and

$$\bar{\Theta}(z) = \int_z^{h_s+h} \Delta_\Theta(z'')\, \mathrm{d}z''. \tag{2}$$

The mean wind components are (U, V, W), with V defined in the downslope direction; (u, v, w) represent the components of turbulent velocity fluctuations. $\bar{\Theta}$ (unit K m) equals Δ_Θ vertically integrated between level z and some level h that is chosen well above the top of the TDL. α is the slope of the surface.

We introduce the following acronyms for the terms in the momentum budget: KAT is the katabatic pressure gradient force (PGF) resulting from a negative temperature perturbation over sloping terrain; LSC represents the large-scale PGF that drives motion in the Ekman layer over flat terrain; THW represents the PGF due to horizontal changes in $\bar{\Theta}$; this term drives, for instance, sea-breeze circulations over flat terrain. ADVH/ADVV are horizontal/vertical advection of momentum that are usually small in Antarctic katabatic winds (Parish and Waight, 1987). COR indicates Coriolis turning and FDIV the vertical divergence of the turbulent momentum flux, which is calculated as a residual term and absorbs model horizontal diffusion and gravity-wave drag. For a more detailed discussion of the East Antarctic TDL momentum budget the reader is referred to Van den Broeke et al. (2002).

3.4. Ensembles and normalized sensitivity

In the following we present averages for two ensembles that are referred to as the *strong vortex* ensemble (July 1983, 1984, 1985, 1986, 1988, 1989 and 1993) and *weak vortex* ensemble (July 1980, 1981, 1982, 1987, 1990, 1991 and 1992). The discriminating parameter is the AAO index, based the first principal component of the 850-hPa extratropical height field (20–90°S) from NCEP/NCAR Reanalysis (Thompson and Wallace, 2000). Note that U_{LSC} in Bin 13 (Fig. 4a) correlates strongly with the AAO index ($r = 0.89$) and would yield the same ensemble partitioning.

3.5. Normalized sensitivity

Model layer 11 is chosen as representative for the large-scale zonal wind speed U_{LSC} outside the influence of the TDL. The height above ground level of this layer is about 6 km over the sea and decreases to about 4 km above the highest domes of the ice sheet in the hybrid sigma coordinate system used in RACMO/ANT1. Figure 4a shows U_{LSC} in five selected bins. Interannual variability is clearly much larger over the ocean than over the ice sheet, with monthly mean values in Bin 13 ranging from 8 to 20 m s^{-1}. Strength and variability of U_{LSC} decrease quickly over the ice sheet.

We define the response factor for Bin X as:

$$\text{RF}_X = \frac{\partial U_{\text{LSC,Bin}\,X}}{\partial U_{\text{LSC,Bin 13}}}. \tag{3}$$

RF_X drops to 0.1 over the highest part of the ice sheet (Fig. 4b) but is significantly different from zero in all bins. Variability of the circumpolar vortex (which is most manifest north of Antarctica) thus influences the free atmosphere zonal wind over the entire East Antarctic ice sheet. We define the *normalized sensitivity* of a parameter in Bin X as its local sensitivity to U_{LSC} multiplied by RF_X. The normalized sensitivity indicates the change that can be expected over East Antarctica per m s^{-1} of vortex strengthening in Bin 13.

4. Vertical profiles in Bin 5 (1750–2250 m asl)

Figure 5 shows composite July vertical potential temperature profiles for Bin 5 (1750–2250 m asl) for weak (open symbols) and strong vortex (filled symbols) ensembles. Dashed lines represent background potential temperature Θ_0. In both ensembles the TDL is ca. 2 km thick and the temperature deficit exceeds

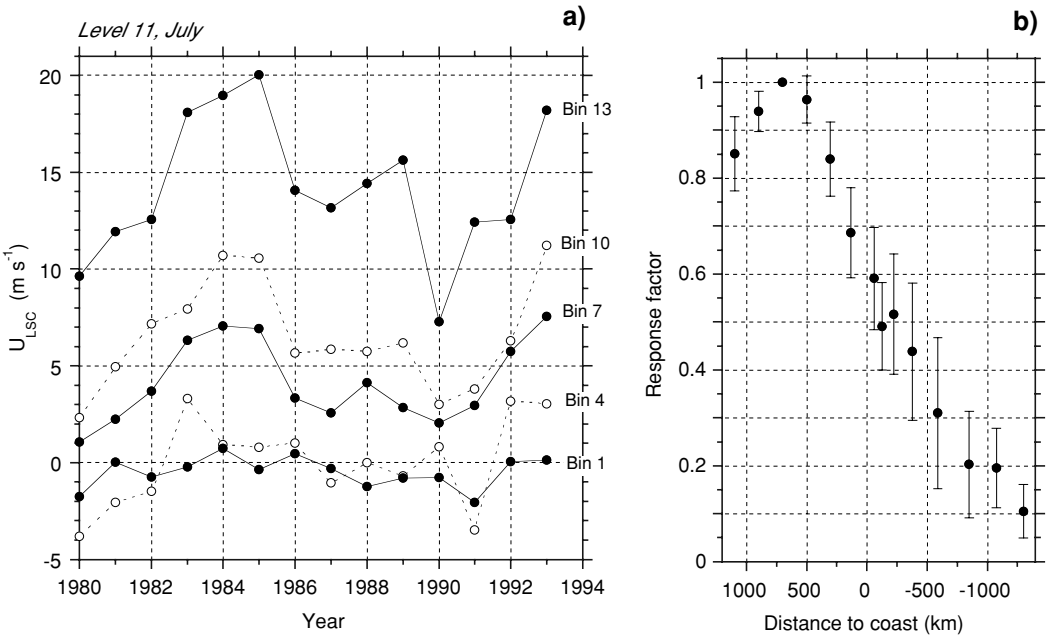

Fig. 4. July mean large-scale zonal wind (model level 11) in selected bins, 1980–1993 (a) and associated response factor (b). Error bars represent one standard error. See text for further explanation.

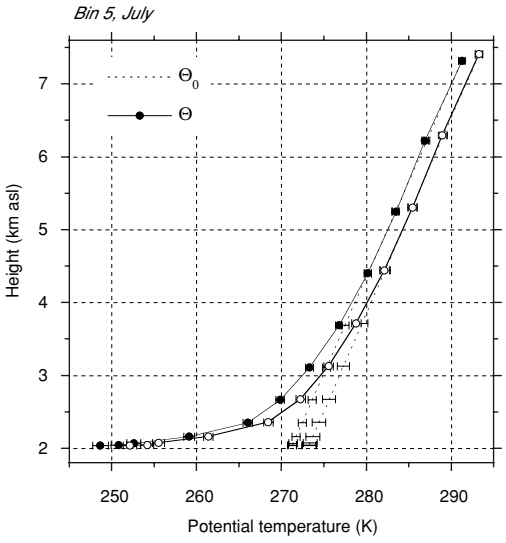

Fig. 5. Bin 5 (1750–2250 m asl), July: average potential temperature Θ (K) for strong vortex ensemble (filled symbols) and weak vortex ensemble (open symbols). Dashed lines indicate background potential temperature Θ_0 (K). Error bars represent one standard error.

20 K at the surface. In strong vortex conditions a 2 K decrease of Θ_0 is seen that is uniform with height and significant at all levels. It is caused by reduced meridional heat exchange and subsequently altered radiation/advection conditions over East Antarctica. In the TDL, an *extra* cooling is found that has a maximum at the surface. This additional cooling is caused by reduced downward mixing of potentially warm air in response to decreased TDL wind speeds (see below). As a result, Δ_Θ at the surface increases from 21 to 22.5 K, i.e. the surface cools by $2.0 + 1.5\,\mathrm{K} = 3.5\,\mathrm{K}$.

Figure 6a shows Bin 5 wind components for weak (open symbols) and strong vortex ensembles (filled symbols). The large-scale wind (U_{LSC}, V_{LSC}) is indicated by dashed lines. In both ensembles U inside the TDL (in an absolute sense) exceeds U_{LSC} owing to the katabatic component (KAT). This causes the characteristic 'nose-shaped' low-level wind speed maximum. However, a very significant part of the near-surface easterlies is ultimately forced by the large-scale pressure gradient, given the surface values of U_{LSC} of 6–8 m s^{-1}. In fact, in this elevation interval the contribution of the downslope large-scale pressure gradient

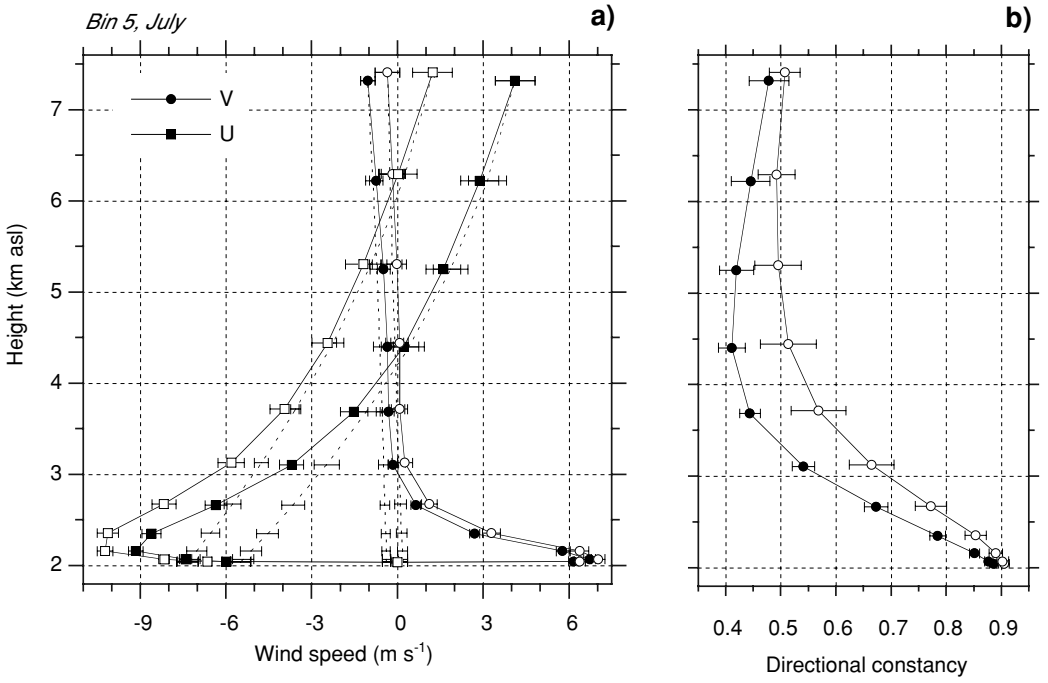

Fig. 6. Bin 5 (1750–2250 m asl), July: average wind components (U, V) for strong vortex ensemble (filled symbols) and weak vortex ensemble (open symbols) (a) and directional constancy (b). Dashed lines indicate large scale wind conmponents (U_{LSC}, V_{LSC}). Error bars represent one standard error.

force ($\mathrm{LSC_d}$) to the total downslope PGF is largest of all bins (Van den Broeke et al., 2002).

In both ensembles, the vertical variation of the large-scale wind vector is due entirely to the cross slope component U_{LSC}. V_{LSC} is weak, which indicates that large-scale air transport across the ice sheet elevation contours is of transient nature only. According to the thermal wind balance this is indicative of a purely downslope directed horizontal background temperature gradient $\partial\Theta_0/\partial y$. This demonstrates that the cooling effect of the East Antarctic ice sheet surface is not confined to the TDL, but also influences the background temperature field Θ_0. A faster decrease of U_{LSC} at lower levels in Fig. 6a indicates larger absolute $\partial\Theta_0/\partial y$ near the surface, so that atmospheric background stability $\gamma_\Theta = \Theta_0/\partial z$ must increase towards the ice sheet interior. The non-zero downslope component V near the surface is forced by surface drag that turns the wind vector in the downslope direction.

Under strong vortex conditions, upper air westerlies increase significantly. The level at which U_{LSC} changes from easterly to westerly is only 2 km above ground level, while it is 4 km in the weak vortex ensemble. This results in a suppressed and lowered easterly wind speed maximum in the TDL. The ensemble difference in U_{LSC} becomes smaller near the surface, indicating that years with a strong vortex have larger $\partial\Theta_0/\partial y$. This means that background cooling is stronger over the East Antarctic ice sheet than in its surroundings, indicative of reduced meridional air exchange under strong vortex conditions (see section 5).

Figure 6b shows ensemble means of directional constancy c_{d}, defined as the ratio of the average absolute to average vector wind speed:

$$c_{\mathrm{d}} = (\bar{u}^2 + \bar{v}^2)^{1/2}/\overline{(u^2 + v^2)^{1/2}}. \qquad (4)$$

c_{d} decreases significantly in the lower troposphere in the strong vortex ensemble. This indicates that the vector mean wind speed decreases less strongly than the absolute mean wind speed, i.e. that wind direction has become more variable. This can be ascribed to the downward displacement of the level where the zonal wind component changes sign, where a minimum in c_{d} is found.

Figure 7 shows vertical momentum balance profiles for the weak (open symbols, dashed lines) and strong

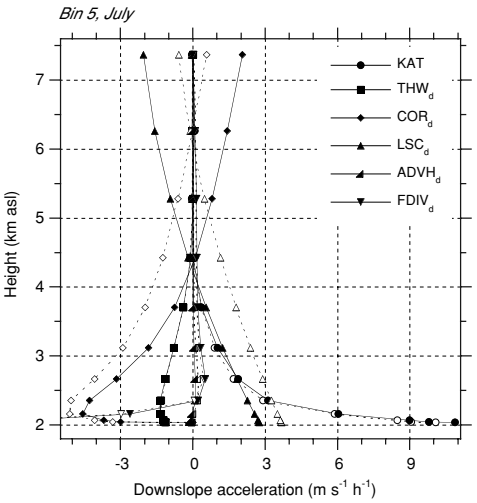

Fig. 7. Bin 5 (1750–2250 m asl), July: average momentum balance terms for strong vortex ensemble (filled symbols) and weak vortex ensemble (open symbols). Error bars represent one standard error.

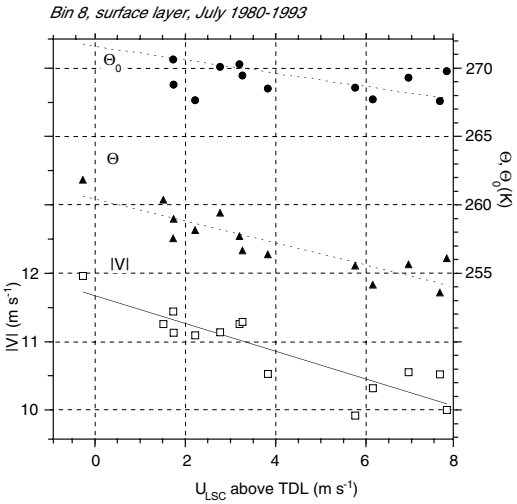

Fig. 8. Bin 8 (150–750 m asl), July, surface layer: correlation of average potential temperature Θ, background potential temperature Θ_0 and wind speed $|V|$ with large-scale zonal wind U_{LSC} (model level 11).

vortex (filled symbols, solid lines) ensembles for July and Bin 5 (1750–2250 m asl). In agreement with Parish and Cassano (2001) $\mathrm{LSC_d}$ is an important contributor to the downslope PGF; at the surface it represents almost 40% of KAT for the weak vortex ensemble and it dominates in the upper TDL, where Δ_Θ becomes quickly smaller. When the vortex is strong, surface $\mathrm{LSC_d}$ decreases and surface KAT increases, so that this contribution drops to 25%. The result is a net decrease of the total downslope PGF, which leads to the weakening of near-surface easterlies, which in turn reduces the absolute magnitude of vertical mixing, $\mathrm{FDIV_d}$.

5. Horizontal profiles in the surface layer

In this section we discuss variability in the surface layer (SL), the lowest model layer at 6–7 m above ground level. The East Antarctic SL is especially interesting because (a) most observations are performed in it (e.g. automatic weather stations, Allison et al., 1993), and (b) the conditions in the SL determine the turbulent exchange of heat, momentum and moisture (mass) with the ice sheet surface.

Figure 8 shows Bin 8 (150–750 m asl) SL potential temperature Θ, background potential temperature Θ_0 and wind speed $|V|$ as a function of local large-scale zonal wind $U_{\mathrm{LSC,Bin5}}$. Clearly, most of the variations in the SL climate are explained by variations in U_{LSC}, with linear correlation coefficients $R = 0.61$ for Θ_0 (significance better than 99%) and $R = 0.88$ for Θ and $|V|$ (significances both better than 99.9%). This shows that the connection between surface layer climate and large-scale circulation as observed and presented in Fig. 2 is also present in RACMO/ANT1, although wind speed variability is smaller than in the observations (Fig. 2). This may well be caused by local topographical features that strongly influence local wind conditions (Mather and Miller, 1967) and that are not resolved by the RACMO/ANT1 topography.

In the following we present the sensitivity of SL variables (level 11) as a function of distance to the coast (DTC, defined negative over the ice sheet). All sensitivities to the local U_{LSC} are normalized by the response factor. This will be referred to as *normalized sensitivity* (see section 3.5), which should give a good estimate of changes one may expect in the East Antarctic SL as a result of changes in the strength of the circumpolar vortex. Note that the significance of the normalized sensitivity can not be greater than the significance of the response factor. In addition to this, the strong and weak vortex ensemble means are presented versus DTC.

Figure 9 shows the normalized sensitivity (a) and ensemble means (b) of SL Θ_0, Θ and Δ_Θ. Θ generally decreases under strong vortex conditions; its sensitivity shows a rather flat minimum from the coast to

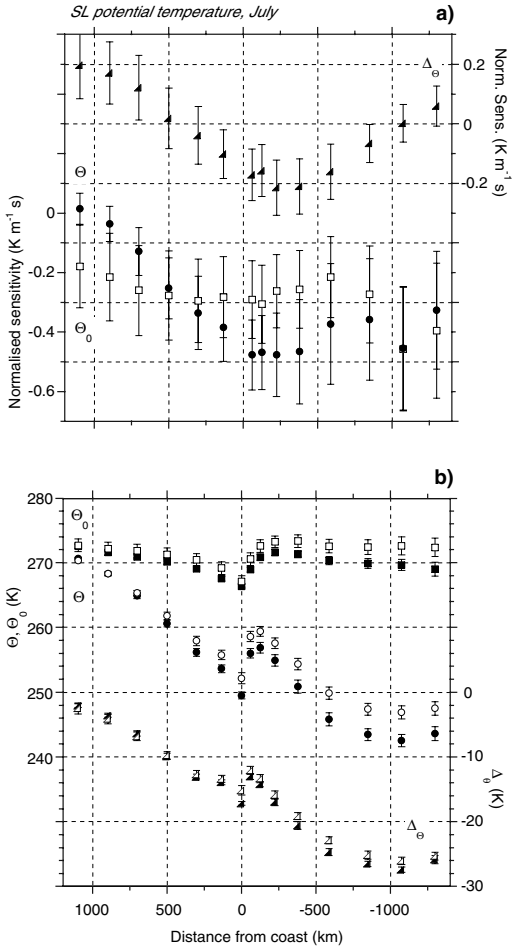

Fig. 9. July, surface layer: (a) normalised sensitivity of SL potential temperature Θ, background potential temperatue Θ_0 and potential temperature perturbation Δ_Θ to changes in the zonal large-scale circulation U_{LSC}. Error bars represent one standard error; (b) potential temperature distribution for strong vortex ensemble (filled symbols) and weak vortex ensemble (open symbols).

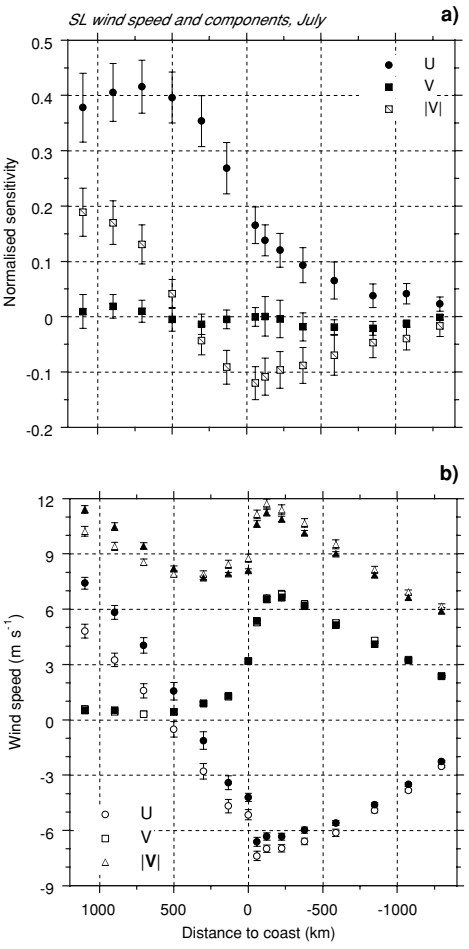

Fig. 10. As Fig. 9, but for SL absolute wind speed and components.

400 km over the ice. In Bin 15 the fixed temperature of the open sea strongly limits the range of Θ. The contribution of Θ_0 and Δ_Θ to SL cooling varies with elevation. All bins show lower Θ_0, with the strongest decrease over the ice sheet interior and a secondary minimum near the grounding line. The sensitivity of Δ_Θ is significantly negative in Bins 5 and 6. We conclude that under strong vortex conditions, SL cooling in the interior of the East Antarctic ice sheet derives almost entirely from changes in Θ_0, while in the elevation interval 1750–3250 m asl about half of the cooling is contributed by Δ_Θ. Over the ocean north of the CPT, Θ_0 decreases but Θ remains nearly constant, so that a positive change of Δ_Θ is found which, however, is not significant.

Figure 10 shows the normalized sensitivity (a) and ensemble means (b) of absolute SL wind speed and components. The cross-slope component *U* shows significant positive sensitivity for the entire domain, except for the highest ice sheet bin, while the downslope component *V* does not change in a significant fashion in any bin. This results in decreased SL easterlies and wind speed over the ice sheet and ocean south of the CPT and increased SL westerlies and wind speed over

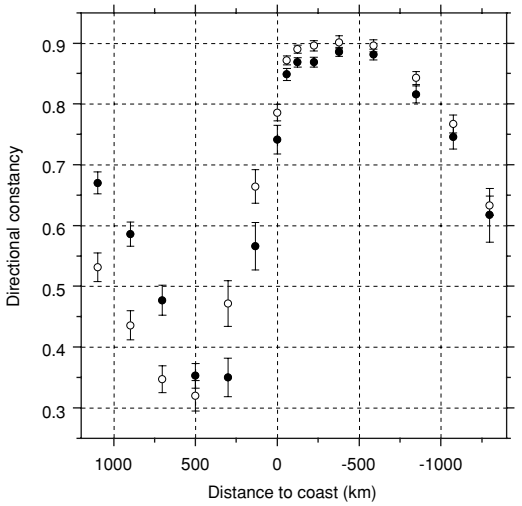

Fig. 11. SL wind directional constancy for strong vortex (open symbols) and weak vortex ensemble (filled symbols).

the ocean north of the CPT. The absolute changes over the ice sheet are small (Fig. 10b) because increased katabatic forcing owing to the increased temperature deficit moderates the response of SL winds (see below). Over the ocean, where katabatic forcing is absent, relative wind changes are more significant.

Figure 11 shows changes of the directional constancy c_d. Not surprisingly, when the vortex is strong, c_d is reduced in regions where easterly surface winds prevail (south of the CPT and over the ice sheet), while an increase is found for the region with prevailing westerlies north of the CPT. Changes over the ice sheet are only significant in the coastal bins where c_d has decreased.

Figure 12 shows sensitivity (a) and composite horizontal profiles (b) of the terms in the SL downslope momentum budget. Over the ice sheet in Bins 4 and 5 changes in LSC_d and KAT balance in first order. The steep coastal ice slopes (Bins 6–8) show large positive sensitivity in KAT, balanced by negative values for THW_d. This balance indicates that strong vortex conditions lead to a more horizontal TDL top, i.e. the trapping of cold air over the coastal ice slopes. The large-scale winds in the coastal TDL are relatively weak, so that cold air from the ice sheet is not removed from the coastal area, providing an effective mechanism for the deceleration of katabatic winds through THW_d. The present results show that this mechanism is enhanced under strong vortex conditions, when the large-

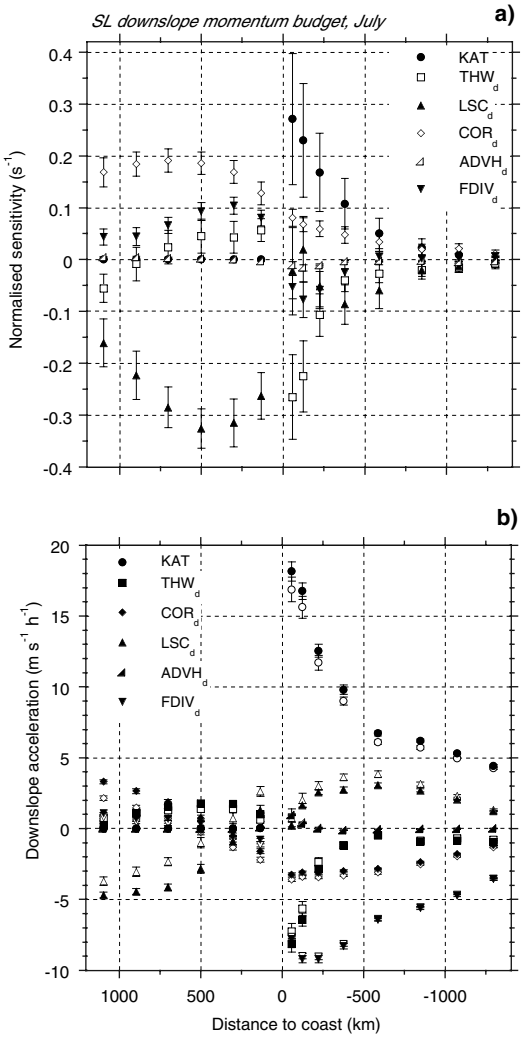

Fig. 12. As Fig. 9, but for SL momentum budget.

scale easterlies south of the CPT become weaker so that the layer of cold air originating from the ice sheet grows even thicker under strong vortex conditions.

Over the ocean, changes in LSC_d are balanced by increased zonal geostrophic winds (COR_d) and the associated increase in surface drag ($FDIV_d$). The increased depth of cold air over the coastal seas enhances northward outflow, so that THW_d also compensates for the decrease in LSC_d, enhancing coastal easterlies south of the CPT and weakening the westerlies north of it.

It was stated earlier that the decreased vertical mixing because of weaker SL winds lead to lower SL

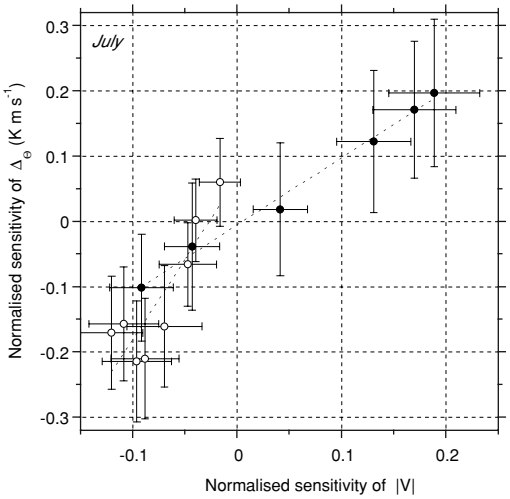

Fig. 13. Normalised sensitivities of surface layer potential temperature deficit Δ_Θ and surface layer wind speed $|V|$. Open symbols: ice sheet bins; Filled symbols: ocean bins.

temperatures through an increased temperature deficit. Figure 13 confirms that a significant correlation exists between the normalized sensitivities of Δ_θ and $|V|$, i.e. the temperature deficit and wind speed in the SL react in a similar fashion to changes in the vortex. This reflects the importance of wind shear generated turbulence on the vertical distribution of temperature in the stable, East Antarctic SL. This will be discussed in more detail in a paper dealing with the heat budget of the East Antarctic ABL. Note that the wind speed range of ice sheet bins in Fig. 13 (open symbols) is much smaller than over sea ice bins (filled symbols). Moreover, over the sea ice the linear correlation goes through $(0, 0)$, while this is not the case for the ice sheet bins. This underscores the importance of the negative feedback from katabatic forcing on SL wind speed sensitivity over the ice sheet.

6. Summary and conclusions

We used data from the regional atmospheric climate model RACMO/ANT1 to study how interannual variability in the strength of the circumpolar vortex influences the surface layer (SL) climate of East Antarctica. In July, when the vortex is strong, we find increased SL westerlies over the ocean north of the circumpolar pressure trough (CPT) and decreased SL easterlies south of it. Over the ice sheet, a significant negative correlation is found of the strength of the vortex with SL potential temperature, in agreement with observations. The signal is composed of two effects: strong zonal flow means less meridional air exchange by the Rossby waves, which leads to lower tropospheric *background* temperatures by 1–3 K over East Antarctica. Secondly, weaker winds in the surface layer generate less downward mixing of warm air in the stably stratified surface layer, so that the temperature deficit near the surface is enhanced. In the ice sheet elevation interval 1750–3250 m asl about half of the cooling comes from the last effect. Under strong vortex conditions the depth of the cold air layer over the coastal sea ice increases, trapping the cold air over the slopes of the coastal ice sheet but at the same time enhancing easterlies over the coastal seas through outflow effects.

In this paper we concentrated on East Antarctica, which shows a relatively uniform response to variations in vortex strength. In a forthcoming paper we will discuss the very different response in the region of the Antarctic Peninsula to changes in the circumpolar vortex.

7. Acknowledgments

Erik van Meijgaard (KNMI) is thanked for model support. The comments of two anonymous reviewers have improved the manuscript. This work is a contribution to the "European Project for Ice Coring in Antarctica" (EPICA), a joint ESF (European Science Foundation)/EC scientific programme, funded by the European Commission under the Environment and Climate Programme and by national contributions from Belgium, Denmark, France, Germany, Italy, the Netherlands, Norway, Sweden, Switzerland and the U K.

REFERENCES

Allison, I., Wendler, G. and Radok, U. 1993. Climatology of the East Antarctic ice sheet (100°E to 140°E) derived from automatic weather stations. *J. Geophys. Res.* **98**, 8815–8823.

Burnett, A. W. and McNicoll, A. R. 2000. Interannual variations in the southern hemisphere winter circumpolar vortex: relationships with the semiannual oscillation. *J. Climate* **13**, 991–999.

Connolley, W. M. 1996. The Antarctic temperature inversion. *Int. J. Climatol.* **16**, 1333–1342.

Doran, P. T., Priscu, J. C., Lyons, W. B., Walsh, J. E., Fountain, A. G., McKnight, D. M., Moorhead, D. L., Virginia, R. A., Wall, D. H., Clow, G. D., Fritsen, C. H., McKay, C. P. and Parsons, A. N. 2002. Antarctic climate cooling and terrestrial ecosystem response. *Nature* **415**, 517–520.

Jones, P. D. 1995. Recent variations in mean temperature and the diurnal temperature range in the Antarctic. *Geophys. Res. Lett.* **22**, 1345–1348.

King, J. C. and Harangozo, S. A. 1998. Climate change in the western Antarctic Peninsula since 1945: observations and possible causes. *Ann. Glac.* **27**, 571–575.

Mahrt, L. 1982. Momentum balance of gravity flow. *J. Atmos. Sci.* **39**, 2701–2711.

Mather K. B. and Miller, G. S. 1967. *Notes on topographic factors affecting the surface wind in* Antarctica, with special reference to katabatic winds and bibliography. *Geophys. Inst. Rep.* UAGR-189, University of Alaska, Fairbanks, 125 pp.

Meehl, G. A., Hurrel, J. W. and Van Loon, H. 1998. A modulation of the mechanism of the semiannual oscillation in the Southern Hemisphere. *Tellus* **50A**, 442–450.

Parish, T. R. and Waight, K. T. 1987. The forcing of Antarctic katabatic winds. *Mon. Wea. Rev.* **115**, 2214–2226.

Parish, T. R. and Bromwich, D. H. 1987. The surface windfield over the Antarctic ice sheets. *Nature* **328**, 51–54.

Parish, T. R. and Cassano, J. J. 2001. Forcing of the wintertime Antarctic boundary layer winds from the NCEP–NCAR global reanalysis. *J. Appl. Meteorol.* **40**, 810–821.

Raper, S. C. B., Wigley, T. M. L., Mayes, P. R., Jones, P. D. and Salinger, M. J. 1984. Variations in surface air temperature. Part 3: the Antarctic, 1957–82. *Mon. Wea. Rev.* **112**, 1341–1353.

Scambos, T. A., Hulbe, C., Fahnestock, M. and Bohlander, J. 2000. The link between climate warming and break-up of ice shelves in the Antarctic Peninsula. *J. Glaciol.,* **154**, 516–530.

Thompson, D. W. J. and Wallace, J. M. 2000. Annular modes in the extratropical circulation. Part I: Month-to-month variability. *J. Climate* **13**, 1000–1016.

Thompson, D. W. J. and Solomon, S. 2002. Interpretation of recent Southern Hemisphere climate change. *Science* **296**, 895–899.

Van den Broeke, M. R. 2000a. The semi-annual oscillation and Antarctic climate, part 5: Impact on the annual temperature cycle as derived from NCEP re-analysis. *Clim. Dynamics* **16**, 369–377.

Van den Broeke, M. R. 2000b. On the interpretation of Antarctic temperature time series. *J. Climate* **13**, 3885–3889.

Van den Broeke, M. R., van Lipzig, N. P. M. and van Meijgaard, E. 2002. Momentum budget of the East-Antarctic atmospheric boundary layer: results of a regional climate model. *J. Atmos. Sci.,* in press.

Van Lipzig, N. P. M. 1999. *The surface mass balance of the Antarctic ice sheet: a study with a regional atmospheric model.* PhD Thesis, Utrecht University, The Netherlands (can be obtained from IMAU, P.O. Box 80005, 3508 TA Utrecht, The Netherlands).

Van Lipzig, N. P. M., van Meijgaard, E. and Oerlemans, J. 1999. Evaluation of a regional atmospheric model using measurements of surface heat exchange processes from a site in Antarctica. *Mon. Wea. Rev.* **127**, 1994–2011.

Van Loon, H. 1967. The half-yearly oscillation in the middle and high southern latitudes and the coreless winter. *J. Atmos. Sci.* **24**, 472–486.

Vaughan, D. G. and Doake, C. S. M. 1996. Recent atmospheric warming and retreat of ice shelves on the Antarctic Peninsula. *Nature* **379**, 328–331.